Realization of a Monolithic High-Reflectivity Cavity Mirror from a Single Silicon Crystal

Frank Brückner,[1] Daniel Friedrich,[2] Tina Clausnitzer,[1] Michael Britzger,[2] Oliver Burmeister,[2] Karsten Danzmann,[2] Ernst-Bernhard Kley,[1] Andreas Tünnermann,[1] and Roman Schnabel[2]

[1]*Institut für Angewandte Physik, Friedrich-Schiller-Universität Jena, Max-Wien-Platz 1, 07743 Jena, Germany*
[2]*Max-Planck-Institut für Gravitationsphysik and Leibniz Universität Hannover, Callinstraße 38, 30167 Hannover, Germany*

We report on the first experimental realization of a high-reflectivity cavity mirror that solely consists of a single silicon crystal. Since no material was added to the crystal, the urgent problem of "coating thermal noise" that currently limits classical as well as quantum measurements is avoided. Our mirror is based on a surface nanostructure that creates a resonant surface waveguide. In full agreement with a rigorous model we realized a reflectivity of $(99.79 \pm 0.01)\%$ at a wavelength of 1.55 μm, and achieved a cavity finesse of 2784. We anticipate that our achievement will open the avenue to next generation high-precision experiments targeting fundamental questions of physics.

Cavity mirrors for laser radiation are essential as heavy test masses of space-time for the new field of gravitational wave astronomy [1,2], as mechanical oscillators for targeting the quantum regime of macroscopic mechanical devices [3–5], and for ultra-high-precision optical clocks designed for researching the nature of fundamental constants [6–8]. Current limitations in all fields are set by the joint problem of lacking appropriate cavity mirror qualities. The purpose of cavity mirrors is to repeatedly retro-reflect laser light such that it constructively interferes with the stored cavity field yielding maximum field amplitudes and providing an output field of highest phase stability. In order to do so cavity mirrors need high reflectivities and a geometrically well-defined surface profile. If the mirror surface shows statistical fluctuations, for example, driven by Brownian motion of the mirror's molecules, the phase fronts of subsequently reflected waves are slightly different and cannot perfectly interfere constructively, which results in a reduced cavity buildup and, most severely, in changes of the phase of the output laser beam. Motions of mirror surfaces, driven by thermal energy, are known as (Brownian) thermal noise and currently a major limiting factor in many research fields targeting fundamental questions of nature as mentioned above [9–11].

The best starting point for the fabrication of low thermal noise mirrors is to employ crystalline materials with high intrinsic mechanical quality factors (Q factors), low thermal expansion coefficients, and low absorption of the laser light, at cryogenic temperatures. A useful summary of thermal noise relations can be found in [11]. Within the past years silicon was found to be a promising candidate [12] with an absorption of probably less than 10^{-8} cm^{-1} at a 1550 nm wavelength [13] and Q factors of 10^9 at cryogenic temperatures [14]. In order to achieve high reflectivities for high-finesse setups dielectric multilayer coatings on the substrate's surface are currently employed, and reflectivities of up to 99.9998% have been demonstrated [15]. However, recent theoretical and experimental re-

search revealed that these coatings reduce the substrate Q factors and, most severely, lead to a strong inhomogeneous dissipation and therefore to a rapidly increasing Brownian thermal noise level [9,16–18]. Thus, besides optimizing multilayer stacks [19] or trading off coherent thermal noise sources [11,20], a coating-free (i.e., monolithic) mirror concept is of enormous interest. Previous published approaches such as corner reflectors [21,22] or whispering-gallery-mode resonators [23,24] are based on total internal reflection and significant optical path lengths inside a substrate giving rise to absorption and thermorefractive noise resulting from a temperature dependent index of refraction.

This work experimentally demonstrates for the first time a monolithic surface mirror [see Fig. 1(a)], i.e., a single piece of monocrystalline silicon with a reflectivity high enough to form a laser cavity with a finesse of almost 3000. The achieved high reflectivity relies on resonant coupling to a guided optical mode of a surface nanostructure [25,26]. Since no material is added to the silicon substrate, the limiting coating Brownian thermal noise as found in Refs. [9,16] is avoided. A coating related reduction of substrate Q factors should also be greatly avoided, as suggested by first experimental results [18]. Our approach uses a broadband guided optical mode and therefore does not increase the interaction length of light with matter thus keeping thermorefractive noise as well as absorption low.

In Figs. 1(b)–1(e) we plot the evolution from previous nonmonolithic to the monolithic guided-mode resonant waveguide grating mirror. We use a simplified ray picture [25] in order to explain how reflectivities close to unity are achieved. The mirror architecture in Fig. 1(b) uses a second material coated on the substrate's surface, and was initially proposed for narrowband optical filters and switching applications in the mid 1980s. It comprises a periodically corrugated high-refractive index layer attached to a low-refractive index substrate. In order to allow for resonant reflection under normal incidence, the corrugation period
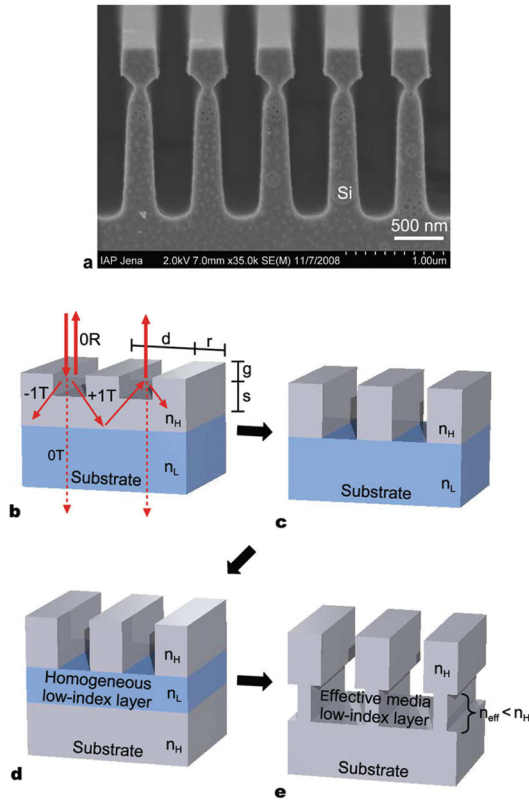
FIG. 1 (color).   Monolithic mirror from a nanostructured single silicon crystal. (a) SEM (scanning electron microscope) cross-sectional view of a 700 nm period T-shaped grating in a silicon bulk substrate that forms the monolithic cavity mirror's surface, efficiently reflecting normally incident light with a wavelength of 1.55 μm. (b) Conventional resonant waveguide grating with a high-index layer corrugated at its surface on top of a low-index substrate. (c) Stand-alone high-index grating ridges corresponding to a zero waveguide layer thickness ($s = 0$ nm). (d) Reduction of the low-index substrate to a thin layer. (e) Monolithic implementation of element (d) by replacing the homogeneous low-index layer by an effective media low-index layer.

must fulfill the following parameter inequalities, which can be derived from the well-known grating equation [27]:

$$d < \lambda \quad \text{(to permit only zeroth order in air)}, \quad (1)$$

$$\lambda/n_H < d \quad \text{(first orders in high-index layer)}, \quad (2)$$

$$d < \lambda/n_L \quad \text{(only zeroth order in substrate)}, \quad (3)$$

where d is the grating period, λ is the light's vacuum wavelength, and n_H and n_L are the higher and lower refractive indices, respectively. In our ray picture, the first diffraction orders ($-1T$, $+1T$) within the high-index layer experience total internal reflection and, thus, can excite resonant waveguide modes propagating along the corrugated high-index layer. In turn, a certain fraction of the light inside the waveguide is coupled out again via the grating to both the transmitted and reflected zeroth order ($0T$, $0R$). If the grating period d, the groove depth g, the grating fill factor f (ratio between ridge width r and grating period d), and the high-index layer thickness s with respect

to the refractive index values of the involved materials are designed properly, all transmitted light can be prompted to interfere destructively, corresponding to a 100% reflectivity. Perfect reflectivity can also be achieved without the homogeneous part of the waveguide layer as proposed and realized in Refs. [27,28], see Fig. 1(c). The low-index substrate which is necessary for total internal reflection can be reduced to a layer [26], see Fig. 1(d). This layer has to have a certain minimum thickness, for which evanescent transmission of the higher orders is still low. Although these approaches reduce the thick multilayer stack of conventional mirrors to a thin layer, at least one additional material is added resulting in an increased mechanical loss.

Eventually, as shown in Fig. 1(e), we recently proposed to replace the remaining low-index layer by an effective low-index layer [29]. This grating layer exhibits the same period but has a lower fill factor (LFF) than the structure on top, and has an effective index $n_{\text{eff}} < n_H$. Since the high fill factor (HFF) grating on top does generate higher diffraction orders, referring to Eq. (2), the realization of the LFF grating as an effective medium without higher diffraction orders, according to Eq. (3), is not obvious [30]. The electric field inside this T-shaped structure can be expressed by discrete grating modes according to the modal method [31]. If the fill factor is sufficiently low the LFF grating only supports the fundamental grating mode, which is related to the zeroth diffraction order in case of a homogeneous layer, whereas the HFF grating indeed allows for higher order modes to propagate. Similar to a conventional homogeneous layer, the remaining fundamental mode can show complete destructive interference for all light transmitted to the LFF grating. Thus, the monolithic structure, as depicted in Fig. 1(e), can reach 100% reflectivity for some wavelength if the fill factors and the groove depths of both gratings meet certain values.

The design parameters of our T-shaped grating were found by rigorously solving the Maxwell equations [32]. We aimed for 100% reflectivity for normal incidence of TM-polarized light (electric field perpendicular to the grating ridges) at 1550 nm. The parameter set was further optimized to get a high first-order diffraction efficiency and, thus, broadband guided optical modes, as well as large parameter tolerances for the fabrication process. The result of our numerical calculations resulted in a grating period of 700 nm and was presented in Ref. [29]. We also rigorously calculated the optical near field distribution of this structure; see the supplementary material [33].

For fabrication, a standard silicon wafer with 100 mm in diameter was thermally oxidized with a 1 μm silica layer and coated with a 80 nm chromium layer, both serving as the mask during silicon etching. After spin coating an electron beam sensitive resist on top, the 700 nm period grating was defined by means of electron beam lithography for an area of 7.5×13 mm^2, aiming at a grating fill factor of 0.56 [29]. The developed binary resist profile was then transferred into the chromium layer and subsequently into the oxidized silica layer as well as the silicon bulk substrate

by utilizing an anisotropic (i.e., binary) inductively cou-
pled plasma (ICP) dry-etching process. Here, the etching
time was adjusted to match the desired groove depth of the
upper silicon grating of about 350 nm. The vertical grating
groove side walls were then covered with a thin chromium
layer by coating the whole device under an oblique angle.
With this technique, the groove side walls were protected
from further ICP etching while the groove bottom re-
mained accessible. A second, but this time isotropic (i.e.,
polydirectional), ICP etching process enabled the undercut
of the upper grating to generate the LFF grating beneath.
Here, a well-balanced ratio between horizontal and vertical
etching rate played a decisive role to supply a sufficiently
low grating fill factor (<0.3) as well as a minimum groove
depth of the lower grating of about 500 nm [29]. Finally,
the etching mask materials (silica, chromium, and resist)
were removed by means of wet chemical etching baring the
monocrystalline silicon structure.

Figure 1(a) depicts an SEM (scanning electron micro-
scope) cross-sectional view on the fabricated mirror sur-
face that has been characterized within this work. As
expected, the shape of the grating ridges was not strictly
rectangular, but it was within the parameter tolerances that
predict high reflectivity [29] (for another SEM, see the
supplementary material [33]).

The first measurement of the mirror's reflectivity was
performed under normal incidence ($0° \pm 1°$) and em-
ployed a fiber-coupled tunable diode laser. The measured
data are shown in Fig. 2 (black curve) and reveal a reflec-
tivity of higher than 91.5% for a rather broad spectral range
from approximately 1.21 to 1.61 μm. The peak reflectivity
is located close to the design wavelength of 1.55 μm with
a value of almost 100%, where a measurement error of
$\pm0.3\%$ needs to be taken into account. The red curve in
Fig. 2 represents a rigorously simulated spectral response
for a grating profile that has been formed by a trapezoidal
fragmentation in order to approximate the real shape (in-
dicated by the sketch on the right-hand side of Fig. 2).

In order to demonstrate the high optical quality of our
mirror we incorporated it as the end mirror in a Fabry-Perot
resonator, see Fig. 3(a). A conventional high quality multi-
layer coated mirror served as the coupling mirror with a
measured power transmittivity of $\tau_1^2 = 200 \pm 20$ ppm.
Note that the monolithic mirror substrate had an unpol-
ished rear surface and could not be used as the coupling
mirror. By measuring the cavity's finesse F, this setup also
enabled us to precisely determine the mirror's reflectivity
under an angle of incidence of precisely zero degree at a
wavelength of 1550 nm. The product of the amplitude
reflectivities $\rho_{12} = \rho_1 \rho_2$ of coupling and end mirror, re-
spectively, can be calculated from a measured finesse as
follows:

$$\rho_{12} = \rho_1 \rho_2 = 2 - \cos\frac{\pi}{F} - \sqrt{\left(\cos\frac{\pi}{F} - 2\right)^2 - 1}. \quad (4)$$

The finesse F is defined as the ratio of free spectral range
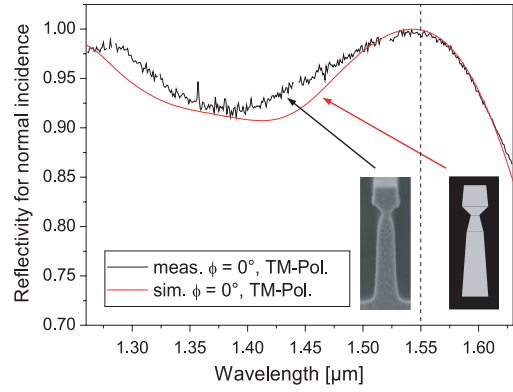(FSR) ν_{FSR} and cavity linewidth $\Delta\nu$ (full width at half

FIG. 2 (color).   Spectral reflectivity. Measured spectral reflec-
tivity of the grating from Fig. 1(a) for normal incidence ($\phi = 0° \pm 1°$) (black curve) and rigorously simulated spectral reflec-
tivity for a grating profile approximating the real shape by a
trapezoidal fragmentation (red curve).

maximum). The FSR was $\nu_{\mathrm{FSR}} = c/(2L) = 6.246 \pm 0.13$ GHz with c the speed of light and $L = 24 \pm 0.5$ mm the distance between both mirrors. In order to
obtain the linewidth of the Fabry-Perot resonator we used
a calibrated tuning of the cavity length around an airy peak.
The calibration was done via frequency markers at
±30 MHz around an airy peak using the Pound-Drever-
Hall (PDH) technique [34], see Figs. 3(a) and 3(b). For
this, a phase modulation was imprinted on the light by an
electro-optical modulator (EOM). The detected signal in
reflection (PD1) was then electronically demodulated by a
local oscillator. We investigated 25 beam positions on the
grating over an area of 4 mm^2 with a beam size radius of
≈ 50 μm. For each position, we did 12 measurements of
the linewidth, which resulted in an averaged value of the
power reflectivity of $\bar{\rho}_2^2 = (99.7682 \pm 0.0095)\%$ for the
overall area. The smallest linewidth was determined to
$\Delta\nu = 2.24 \pm 0.07$ MHz [see Fig. 3(b)]. Hence, the finesse
was found to be $F = 2784 \pm 100$, which corresponds to a
waveguide grating power reflectivity of $\rho_2^2 = (99.7945 \pm 0.0086)\%$, referring to Eq. (4) (for further information, see
the supplementary material [33]). Because of the unpol-
ished back side of the substrate we could only set a lower
limit on the transmission by power measurements of $\tau_2^2 \geq 230 \pm 20$ ppm and, hence, an upper limit on optical losses
due to absorption and scattering of 1820 ± 110 ppm.

The optical reflectivity measured here is, to the best of
our knowledge, the highest resonant reflection ever real-
ized. The measured reflectivity of slightly below unity is
attributed to deviations from the design parameters. How-
ever, it is in very good agreement with our rigorous model
based on Maxwell equations that takes these deviations
into account (Fig. 2). Please note that the same simulation
predicts a reflectivity maximum for about 1.543 μm. A
verification in our cavity setup was not possible since the
laser source was not tunable to this wavelength.

The reflectivity, as demonstrated here, in principle al-
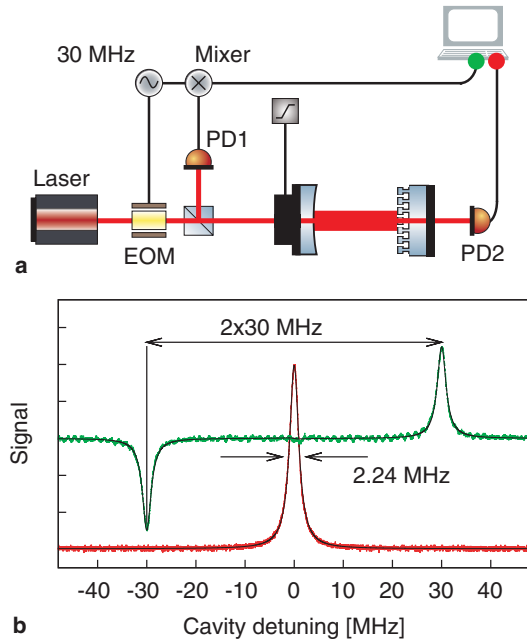lows for a coating-free linear cavity with a finesse of

FIG. 3 (color). High-finesse cavity setup with monolithic end
mirror. (a) Experimental setup for the characterization of the
waveguide grating as a cavity end mirror. Electro-optical modu-
lator (EOM), photodiode (PD). (b) Scan over one cavity reso-
nance (airy) peak (red line) with a linewidth of 2.24 MHz
measured in transmission (PD2), corresponding to a cavity
finesse of 2784 and a power reflectivity of the monolithic mirror
of 99.79%. The cavity detuning was calibrated via the demodu-
lated signal (frequency markers at ± 30 MHz, green line) in
reflection of the cavity (PD1) that was generated with the
PDH technique. Fitted theoretical lines are in black.

≈ 1500, which already reaches the regime of finesse values
used in gravitational wave detectors. For example, the
advanced LIGO Fabry-Perot arm cavities are being de-
signed for a finesse of a few hundred. Note that our
technique can also be adapted to substrates with large radii
of curvature, as required for long arm cavities. Our dem-
onstrated mirror quality may also be already sufficient to
provide an impact towards reaching the quantum regime of
micromechanical oscillators. In Ref. [3] optical cooling of
such an oscillator down to 135 mK was achieved with a
finesse of only 200. Our demonstrated cavity linewidth of
2.24 MHz is significantly smaller than many typical fun-
damental oscillator frequencies and the so-called good
cavity regime can be reached [4]. Note that the cavity
linewidth can be further reduced by increasing the cavity
length. For applications in reference cavities and optical
clocks [7,8] the reflectivities should be further increased
beyond the value demonstrated here, however, we expect
that indeed considerable improvements towards a perfect
reflectivity are possible with improved lithography and
etching technologies. Having demonstrated the first mono-
lithic surface mirror ever, our future work now aims for the
realization of even higher reflectivities and for an *in situ*
experimental confirmation that the thermal noise of our

mirror is for fundamental reasons much lower than any
other high-reflectivity mirror concept.

[1] P. Aufmuth and K. Danzmann, New J. Phys. **7**, 202 (2005).
[2] J. R. Smith *et al.* (LIGO Scientific Collaboration),
Classical Quantum Gravity **26**, 114013 (2009).
[3] D. Kleckner and D. Bouwmeester, Nature (London) **444**,
75 (2006).
[4] A. Schliesser *et al.*, Nature Phys. **5**, 509 (2009).
[5] H. Müller-Ebhardt *et al.*, Phys. Rev. Lett. **100**, 013601
(2008).
[6] Th. Udem, R. Holzwarth, and T. W. Hänsch, Nature
(London) **416**, 233 (2002).
[7] B. C. Young *et al.*, Phys. Rev. Lett. **82**, 3799 (1999).
[8] C. Braxmaier *et al.*, Phys. Rev. D **64**, 042001 (2001).
[9] Y. Levin, Phys. Rev. D **57**, 659 (1998).
[10] V. B. Braginsky, M. L. Gorodetsky, and S. P. Vyatchanin,
Phys. Lett. A **264**, 1 (1999).
[11] M. L. Gorodetsky, Phys. Lett. A **372**, 6813 (2008).
[12] S. Rowan *et al.*, Proc. SPIE Int. Soc. Opt. Eng. **4856**, 292
(2003).
[13] M. A. Green and M. J. Keevers, Prog. Photovolt. Res.
Appl. **3**, 189 (1995).
[14] D. F. McGuigan *et al.*, J. Low Temp. Phys. **30**, 621 (1978).
[15] G. Rempe *et al.*, Opt. Lett. **17**, 363 (1992).
[16] G. M. Harry *et al.*, Classical Quantum Gravity **19**, 897
(2002).
[17] E. D. Black *et al.*, Phys. Lett. A **328**, 1 (2004).
[18] R. Nawrodt *et al.*, New J. Phys. **9**, 225 (2007).
[19] J. Agresti *et al.*, Proc. SPIE Int. Soc. Opt. Eng. **6286**,
628608 (2006).
[20] H. J. Kimble, B. L. Lev, and J. Ye, Phys. Rev. Lett. **101**,
260602 (2008).
[21] G. Cella and A. Giazotto, Phys. Rev. D **74**, 042001 (2006).
[22] S. Goßler *et al.*, Phys. Rev. A **76**, 053810 (2007).
[23] A. B. Matsko *et al.*, J. Opt. Soc. Am. B **24**, 1324 (2007).
[24] I. S. Grudinin, V. S. Ilchenko, and L. Maleki, Phys. Rev. A
74, 063806 (2006).
[25] A. Sharon, D. Rosenblatt, and A. A. Friesem, J. Opt. Soc.
Am. A **14**, 2985 (1997).
[26] C. F. R. Mateus *et al.*, IEEE Photonics Technol. Lett. **16**,
1676 (2004).
[27] A. Bunkowski *et al.*, Classical Quantum Gravity **23**, 7297
(2006).
[28] F. Brückner *et al.*, Opt. Express **17**, 163 (2009).
[29] F. Brückner *et al.*, Opt. Lett. **33**, 264 (2008).
[30] P. Lalanne and D. Lemercier-Lalanne, J. Mod. Opt. **43**,
2063 (1996).
[31] L. C. Botten *et al.*, Opt. Acta **28**, 413 (1981).
[32] M. G. Moharam and T. K. Gaylord, J. Opt. Soc. Am. **71**,
811 (1981).
[33] See supplementary material at http://link.aps.org/
supplemental/10.1103/PhysRevLett.104.163903 for near
field calculations and an additional SEM.
[34] R. W. P. Drever *et al.*, Appl. Phys. B **31**, 97 (1983).